

Telemetric Technique for Wireless Strain Measurement From an Inkjet-Printed Resistive Sensor

Michele Bona, Mauro Serpelloni, *Member, IEEE*, Emilio Sardini, *Member, IEEE*, Cristian O. Lombardo, and Bruno Andò, *Senior Member, IEEE*

Abstract—Strain monitoring allows obtaining critical information regarding the conditions of several systems. It would help, for example, to avoid possible structural damages. However, not all the existing devices are suitable to accomplish this task for a great number of applications, because of the characteristics of measurement environment, which prevent the use of batteries or wired connections. The use of telemetric devices may overcome these limitations, since they rely on the magnetic coupling between two inductors for wireless sensor supply and data transmission. The work treated in this paper presents a technique that permits us to calculate the output of a resistive strain gauge from a measurement of system impedance phase performed at a specific frequency, when distance between the inductors is fixed. We validated the method using a real device working with a low-cost sensor fabricated through inkjet-printing technology on a flexible substrate. We applied successive deformations, until 1% of sensor length at rest position. Calculated strain presents a percentage deviation from measured values going from 0.7% to 7%, whereas the highest uncertainty is 0.02% of sensor length at rest. Experimental results put in evidence, on one hand, the potential of inkjet printing to fabricate valid sensing elements and, on the other hand, that the proposed approach is successful in strain estimation.

Index Terms—Impedance phase, inkjet-printed sensor, strain measurement, telemetric device.

I. INTRODUCTION

IN RECENT years, an increasingly great number of research activities have focused on structural health monitoring field [1], which implies the use of current technologies to assess the actual condition of systems like civil buildings, bridges, power stations, aircrafts [2], and other kinds of vehicles [3]. In fact, damages due to episodic events (such as earthquakes), or progressive degradation caused by weather, aging, stress, and fatigue on construction materials [4], could lead to failures that represent a threat for human safety and require huge amounts of money to be addressed.

Manuscript received May 19, 2016; revised August 10, 2016; accepted August 16, 2016. The Associate Editor coordinating the review process was Dr. Salvatore Baglio.

M. Bona, M. Serpelloni, and E. Sardini are with the Department of Information Engineering, University of Brescia, 25123 Brescia, Italy (e-mail: mauro.serpelloni@unibs.it).

C. O. Lombardo and B. Andò are with the Department of Electric, Electronics and Computer Engineering, University of Catania, 95124 Catania, Italy (e-mail: bruno.ando@dieci.unict.it).

Color versions of one or more of the figures in this paper are available online at <http://ieeexplore.ieee.org>.

Digital Object Identifier 10.1109/TIM.2016.2607958

Several methods have been investigated to acquire information on system conditions. Electromechanical impedance detection and acoustic and optical techniques represent some examples [1]. Among all the monitored magnitudes, strain is one of the most common, since it can provide indications about loads borne by the structures [2]. Furthermore, strain measurement is not limited to this field; in fact, it is also a task widespread in medical applications. For instance, flexible strain sensors were used to estimate wrist joint angle in [5]. Reference [6] presents a passive instrument attached to an orthopedic implant to measure its deformation. Reference [7] illustrates a device that monitors bladder volume in patients suffering from urinary dysfunctions. Finally, [8] describes an implantable system designed to collect information about bone strain during daily activities.

The literature cites different instruments employed to measure strain, relying on various operating principles. Examples touch piezoelectric [9], [10], electroluminescent [11], and optical fiber sensors [12], patch antennas [2], and strain gauges, either resistive [13], [14] or capacitive [4], [7]. However, many existing devices have features unsuitable for the accomplishment of this task where measurement environment is hermetic and/or presents harsh characteristics. For instance, the exploitation of elements like batteries and wired connections has to be avoided if the environment has no access points from the outside or in the case of implanted devices. In fact, periodic replacement of any components would be very difficult to achieve. Furthermore, dimensions and costs should be limited, especially if measurement is performed by more sensors from multiple positions at a time.

The use of telemetric systems is a low-cost solution that could overcome these limitations. In such structures, strain sensor is connected to an inductor, forming a completely passive sensing circuit to be inserted inside the environment. A readout unit provides wireless power supply to the sensor from the outside, and obtains measurement information from it, through another inductor that magnetically couples with the first one. In this way, sensor needs neither cables nor batteries to work, and data elaboration is performed entirely by readout conditioning electronics [15], [16].

Considering an *LC* oscillator circuit with a capacitive [17] or inductive [18] sensing element is the most common approach in telemetric system design. The corresponding measurement principle relies on detecting a shift of circuit resonant

frequencies, consequent to strain change. Specific analytical techniques have been developed, which permit to calculate sensor output starting from system frequency response, which can be evaluated through a study of its electrical impedance at readout unit terminals (i.e., outside measurement environment). Reference [19] provides an example for devices operating with capacitive sensors. However, an approach based on resonance identification requires the continue execution of a frequency sweep, with a consequent increase in detection time and complexity of electronic circuits.

Although the most part of the components in a telemetric system is fabricated through ordinary printed circuit board (PCB) techniques, new ways have been investigated, especially for realizing passive elements. Among these, inkjet-printing technology is playing an important role, since very different electronic devices are prototyped and manufactured with the same easy procedure. In fact, a common office printer is adapted to deposit a conductive ink on a substrate, following a proper pattern previously drawn with a CAD software [15]. Unlike traditional photolithographic methods, neither masks nor complex post-treating phases are required. This permits to save time, materials, and money [14], [20]. Resulting components are characterized by satisfying resolution and reproducibility [14], [20]. Furthermore, inkjet printing allows implementing a combination of multiple solutions. Indeed, different inks are used, like those based on metal nanoparticles (e.g., silver [14], [21], [22]) and polymers, such as poly (3,4-ethylen dioxythiophene)-poly (styrenesulfonate), better known as PEDOT-PSS [23]. In addition, various substrates are considered, both rigid and flexible [20]. Particular attention is focused on the latter, like polyethylene terephthalate (PET) [14], [15] and paper [21], [22], because they are also suitable for applications in which surfaces are not plane. Reference [24] gives an example of an inkjet-printed sensing circuit for a telemetric device.

Starting from the aforementioned points, the work treated in this paper proposes a measurement technique that permits us to calculate the strain applied to a system through a telemetric device, but in a way different from the approach adopted when working with capacitive or inductive sensors. In fact, a resistive strain gauge is used, whose value is calculated from an impedance phase measurement in a particular frequency interval. Andò *et al.* [15] worked with a device that presented a sensor realized through inkjet printing. They analyzed its impedance behavior during the application of increasing strain values. The results confirmed what was expected from theory and they permitted to identify a causal link between strain and impedance. In this paper, we describe how we exploited those achievements to represent such a relationship through mathematical formulas, which are the basis for the proposed technique. Furthermore, we illustrate how the method was validated through tests on a real device.

II. TELEMETRIC MEASUREMENT TECHNIQUE

A. Theoretical Background

Fig. 1 proposes a schematic of a telemetric system working with a resistive strain gauge, together with the equivalent

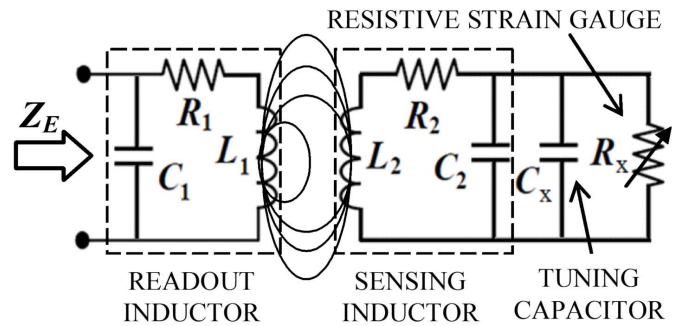


Fig. 1. Circuit representation of a telemetric system working with a resistive strain gauge.

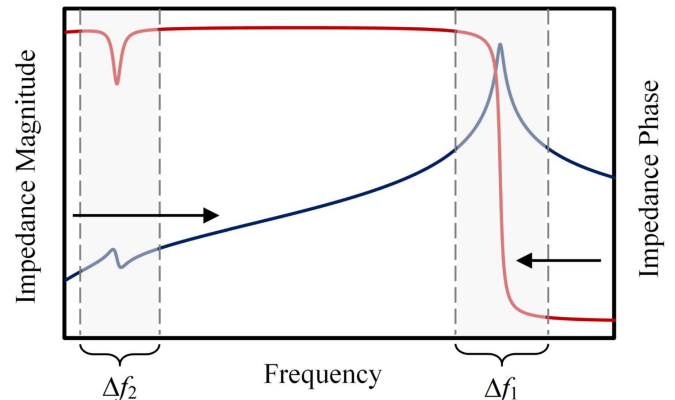


Fig. 2. Qualitative graphs of system impedance magnitude and phase as functions of frequency.

electrical parameters of its elements. It models a simple case, in which there is one inductor connected to readout unit (called “readout inductor”) and coupled with a single sensing circuit. Actually, a real telemetric system could be characterized by multiple readout inductors interfaced with more sensing circuits. They can be combined in series or in parallel to increase system reliability. However, we chose this scheme in order to base our mathematical analysis on an easier model. Looking at Fig. 1 from left to right, readout inductor is represented by an equivalent circuit made of the series between inductance L_1 and resistance R_1 , in parallel with capacitance C_1 [19]. The same condition is valid for the inductor joined to resistive sensor, called “sensing inductor,” when considering parameters L_2 , R_2 , and C_2 . A capacitor C_x can be added in parallel to this component to tune its resonant frequency. Finally, sensor is described by variable resistance R_x , whose value changes according to detected strain.

System impedance at readout unit terminals Z_E depends on these circuit elements. Fig. 2 shows qualitative trends of its magnitude and phase, as functions of frequency. It highlights two intervals. The left one contains local maxima and minima influenced mainly by sensing inductor resonance [19] and, thus, on sensing circuit parameters. It is called Δf_2 . On the contrary, impedance behavior within the right interval Δf_1 depends mostly on the equivalent elements of readout inductor [19]. Therefore, we addressed our attention on Δf_2 , where Z_E is more sensitive to R_x changes than within Δf_1 .

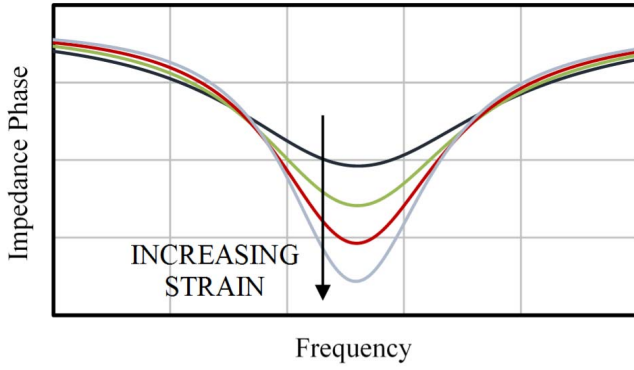


Fig. 3. Qualitative graphs of system impedance phase as a function of frequency, when strain increases. They reflect the results obtained in [15].

Andò *et al.* [15] examined the variations of impedance magnitude and phase due to strain change, within interval Δf_2 . In particular, they focused on phase trend. Fig. 3 reports its qualitative graphs. Two aspects should be highlighted. First, if strain increases, then phase minimum (which is also the most sensitive point) becomes more pronounced, since R_x augments as well. Therefore, they were able to identify an empirical link between sensor output and that function. Second, the results from [15] and Fig. 3 show how there is no variation in the frequency of phase minimum f_{\min} or, at least, change is so limited that it could be neglected. Fonseca *et al.* [25] demonstrated that such a frequency could be identified by the following expression:

$$f_{\min} \cong \frac{1}{2\pi\sqrt{L_2 C_p}} = f_{\text{res}} \quad (1)$$

where C_p represents a capacitance equal to the sum between C_2 and C_x , if distance between the inductors is sufficiently great. f_{res} defines sensing inductor resonant frequency, with the additional contribution given by C_x . Thus, we investigated the possibility of finding a technique based on phase measurement at that particular point.

B. Mathematical Analysis

Equation (2) represents impedance phase mathematical function for the telemetric system shown in Fig. 1. It directly expresses how its parameters (in particular, sensor resistance) influence phase trend

$$\begin{aligned} \angle Z_E(f) = & \frac{\pi}{2} - \text{atan2} \left[\frac{2\pi(L_2 + R_x C_p R_2)f}{R_2 + R_x - 4\pi^2 R_x C_p L_2 f^2} \right] \\ & + \text{atan2} \left[\frac{2\pi(L_1 L_2 - L_2 \beta + R_x C_p L_1 R_2)f}{L_1(R_2 + R_x) - 4\pi^2 R_x C_p L_2(L_1 - \beta)f^2} \right] \end{aligned} \quad (2)$$

where all variables were defined earlier, except parameter β , which takes into account the effects of a variation in magnetic flow exchanged between readout and sensing inductors and, therefore, depends on their relative distance. Its role and how it can be calculated will be explained later.

We found the expression of phase at f_{res} , by substituting (1) into (2). We called it φ

$$\varphi = \angle Z_E(f = f_{\text{res}}). \quad (3)$$

By developing (2) and considering (3), we obtained

$$\tan(\varphi) = \frac{\frac{C_p}{L_2} L_1 R_2^2 R_x^2 + 2L_1 R_2 R_x + \frac{L_2}{C_p} (L_1 - \beta) + L_1 R_2^2}{\sqrt{\frac{C_p}{L_2} R_2 R_x^2 \beta} + \sqrt{\frac{L_2}{C_p} \beta (R_2 + R_x)}}. \quad (4)$$

Then, (4) was rearranged to isolate sensor resistance, leading to a second-order equation in the variable R_x

$$\begin{aligned} & \left[\sqrt{\frac{C_p}{L_2} R_2 \beta \tan(\varphi) - \frac{C_p}{L_2} L_1 R_2^2} \right] R_x^2 \\ & + \left[\sqrt{\frac{L_2}{C_p} \beta \tan(\varphi) - 2L_1 R_2} \right] R_x \\ & + \left[\sqrt{\frac{L_2}{C_p} R_2 \beta \tan(\varphi) - \frac{L_2}{C_p} (L_1 - \beta) - L_1 R_2^2} \right] = 0 \end{aligned} \quad (5)$$

whose acceptable solution is

$$R_x = \frac{2L_1 R_2 - \sqrt{\frac{L_2}{C_p} \beta \tan(\varphi) + \sqrt{\Delta}}}{2\sqrt{\frac{C_p}{L_2} R_2} \left[\beta \tan(\varphi) - \sqrt{\frac{C_p}{L_2} L_1 R_2^2} \right]} \quad (6)$$

where Δ is the determinant of (5). Equation (6) is the analytical relation linking R_x and phase measurement at f_{res} . It allows calculating the former starting from the latter. Performing phase readings at a constant frequency eliminates the necessity of studying the entire impedance spectrum through a complete frequency sweep, leading to savings in measurement time and electronics complexity.

The other circuit elements indicated in Fig. 1 are known. In fact, inductors parameters depend on their geometries [26] and they can be measured, whereas tuning capacitor C_x is chosen during system design process. The only term still undefined is β , which depends on the distance between the inductors. Anyway, the proposed method aims at addressing situations in which strain gauge stays in a point stressed by deformations, whereas inductors remain at a fixed position during the measurement procedure. Examples could regard the monitoring of a cantilever bending and a deformation of a specific point of interest inside a wall, or the measurement of a joint flexion/extension. Therefore, β remains constant. We found a way to obtain its value indirectly, i.e., by reading impedance phase when strain gauge is at rest position (which is a known condition, since we have sensor behavior curve, see Section III) and applying the following expression:

$$\beta = \frac{\frac{C_p}{L_2} L_1 R_2^2 R_{x,0}^2 + 2L_1 R_2 R_{x,0} + \frac{L_2}{C_p} L_1 + L_1 R_2^2}{\sqrt{\frac{C_p}{L_2} R_2 R_{x,0}^2 \tan(\varphi_0) + \sqrt{\frac{L_2}{C_p} (R_2 + R_{x,0}) \tan(\varphi_0) + \frac{L_2}{C_p}}} \quad (7)$$

where $R_{x,0}$ is the sensor resistance at rest position, whereas φ_0 is the corresponding phase read at f_{res} . Equation (7) was achieved by simply reordering (4) in order to isolate the term β . In this way, we implement a single-point system calibration, prior to begin the real measurement procedure.

TABLE I
STRAIN GAUGE CHARACTERISTICS

Property	Symbol	Value (unit)
sensor length at rest position	l_0	27 (mm)
sensor width at rest position	w_0	20 (mm)
tracks width	r	200 (μm)
tracks spacing	s	300 (μm)
sensor resistance at rest position	$R_{x,0}$	4.5 (k Ω)

III. EXPERIMENTAL ANALYSIS

We carried out an experimental analysis to validate the effectiveness of the proposed technique, in particular for the applications requiring the exploitation of low-cost single-use components. For this reason, we chose a telemetric device working with a resistive inkjet-printed sensor.

A. Inkjet-Printed Strain Gauge

The considered strain gauge was fabricated by depositing droplets of silver nanoparticles-based ink Metalon JS-015, commercialized by NovaCentrix, on a 200- μm -thick PET substrate, with a low-cost piezoprinter produced by EPSON. Reference [14] reports some tables in which the main properties of used ink and substrate are listed, whereas Table I includes sensor characteristics. The corresponding pattern was drawn with a CAD software, by setting tracks' width and spacing in a way to guarantee the maximum number of tracks present in the given surface, in order to increase sensor resistance. At the same time, constraints imposed by low-cost inkjet-printing technology were taken into consideration. Indeed, adopting a lower spacing would increase the risks of short circuits [14]. Finally, two pieces of adhesive copper tape were attached to proper points in order to allow for electric contacts. We measured sensor resistance at rest position with Agilent 34401A digital multimeter.

We used the same strain gauge during the entire analysis, since our final goal was measurement method validation. Furthermore, [14] already provides some information on the repeatability of the manufacturing process followed to fabricate our sensor, whose study is beyond the scope of this paper. That reference describes how several strain gauges with certain geometric characteristics were examined. A maximum standard deviation on $R_{x,0}$ of less than 3% was found. Thus, it demonstrates how inkjet-printing technology is capable of fabricating components with a satisfying reproducibility.

We repeated the measurements already carried out in [15]. We used this strain gauge alone, in order to acquire some preliminary information about its behavior, to be kept as a reference for evaluating the proposed method. We exploited the experimental setup shown in Fig. 4. It is a structure designed to clamp sensor PET substrate to two supports. Indeed, PET substrate constitutes a mechanical support for the sensor by itself. Therefore, it does not need to be attached to an external body to be put into operation. We clamped one of sensor edges (i.e., that with electric contacts) to the first support, which is fixed, whereas the other edge was

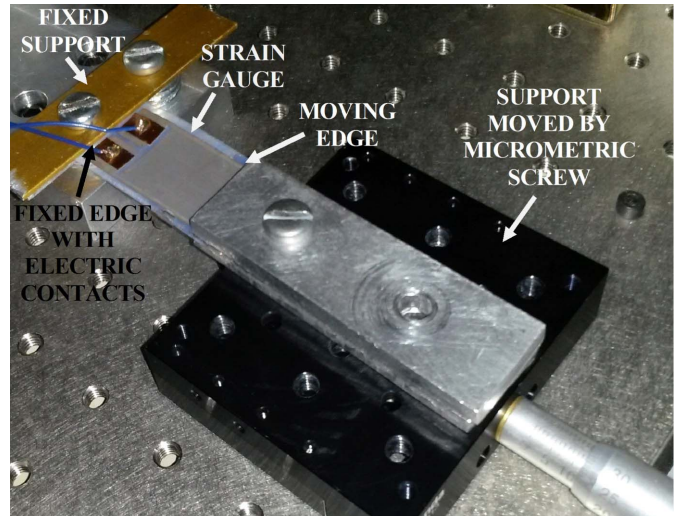


Fig. 4. Fixing structure used for strain application to the sensor.

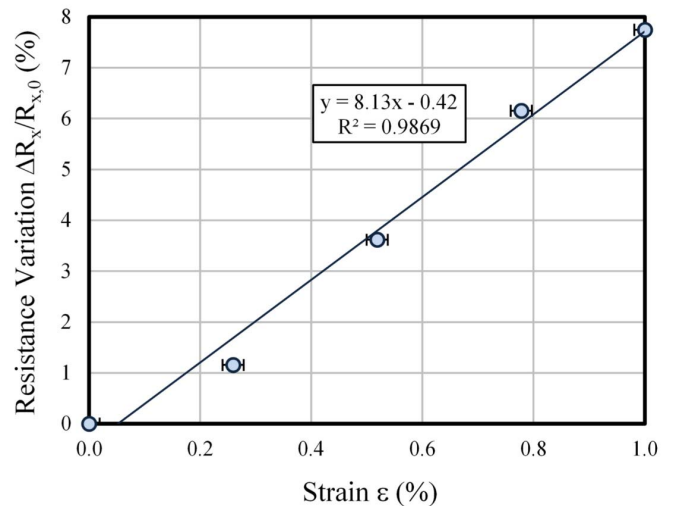


Fig. 5. Sensor resistance variation with respect to its value at rest position, as a function of applied strain.

blocked to the second support, which could move thanks to a micrometric screw. We applied a pulling force along the sensor longitudinal axis by moving the second support, in order to achieve incremental strain levels of about 0.25% of its length at rest, up to a deformation of about $0.01l_0$ (or, in an equivalent way, $10000 \mu\epsilon$), which is close to the limit of sensor elastic deformation domain. At each strain step, we maintained the reached position for few minutes, before increasing the applied force. We implemented such a test protocol since we aimed to simulate the progressively increasing deformations acting on systems over time, which could lead to damages on them. During the entire test, multimeter acquired sensor output with a sampling period of 4 s and sent these data to a laptop.

Fig. 5 shows what we obtained from the analysis of strain gauge behavior. It represents percentage resistance variation with respect to its value at rest position $\Delta R_x/R_{x,0}$ as a function of applied strain ϵ (derived from reading screw graduated scale). We found that R_x increased at a rate of about 2% with respect to its initial value for a single strain interval, leading to an estimated gauge factor equal to

TABLE II
INDUCTORS' CHARACTERISTICS

Property	Symbol	Value (unit) Readout Inductor	Value (unit) Sensing Inductor
Geometric characteristics			
outer side	d_{out}	50 (mm)	27 (mm)
inner side	d_{in}	27 (mm)	5 (mm)
number of windings	N	28	27
windings width	r	150 (μm)	200 (μm)
windings spacing	s	300 (μm)	250 (μm)
Electrical characteristics			
equivalent inductance	L_{ser}	46.9 (μH)	11.9 (μH)
equivalent resistance	R_{ser}	35.0 (Ω)	9.2 (Ω)
equivalent capacitance	C_{par}	3.1 (pF)	1.6 (pF)

about eight, as seen from the y -axis full scale and linear regression angular coefficient. In fact, this trend was maintained along all the examined deformation ranges, with a good linearity (coefficient of determination R^2 is close to 0.99). Gauge factor is quite high, but still in the range of values already found from similar sensors in [14], [15], and [27]. Furthermore, maximum measured uncertainty on $\Delta R_x/R_{x,0}$ is only 0.015%, if considering a 99% confidence interval (CI). Indeed, vertical error bars in Fig. 5 representing the corresponding standard deviation are not visible. This demonstrates once again how an inkjet-printed sensor could be an effective alternative to devices fabricated through traditional technologies.

B. Inductors and Tuning Capacitor

Readout and sensing inductors are planar square spirals that were fabricated through PCB techniques on a rigid FR4 substrate. Table II reports their geometric and electrical characteristics. It should be noted that sensing inductor outer side is equal to readout inductor inner one. This design trick permits to keep to a lower value the parasitic capacitance induced by the electric field created when inductors are coupled, if they are positioned in such a way to be parallel and coaxial [19]. Then, their electrical properties correspond to the parameters of the equivalent circuit used to represent them, as introduced in Section II. Therefore, values assumed by inductance L_{ser} , resistance R_{ser} , and capacitance C_{par} are attributed to L_1 , R_1 , and C_1 for readout inductor and L_2 , R_2 , and C_2 for sensing inductor (see Fig. 1), respectively. We obtained them with an HP4194A impedance analyzer.

Finally, we added a commercial capacitor in parallel to sensing inductor, to act as tuning capacitance C_x . We chose a component equal to 564 pF, in order to set frequency interval Δf_2 around a lower value, i.e., 2 MHz in this case.

C. Experimental Setup and Measurement Procedure

Fig. 6 illustrates a scheme of the setup used to carry out our experimental analysis. We put inkjet-printed strain gauge in the fixing system shown in Fig. 4. However, its terminals were connected to sensing inductor and tuning capacitor C_x , rather than directly to Agilent 34401A multimeter. We positioned sensing inductor in front of readout inductor, at a relative distance fixed to 15 mm, through a mechanical

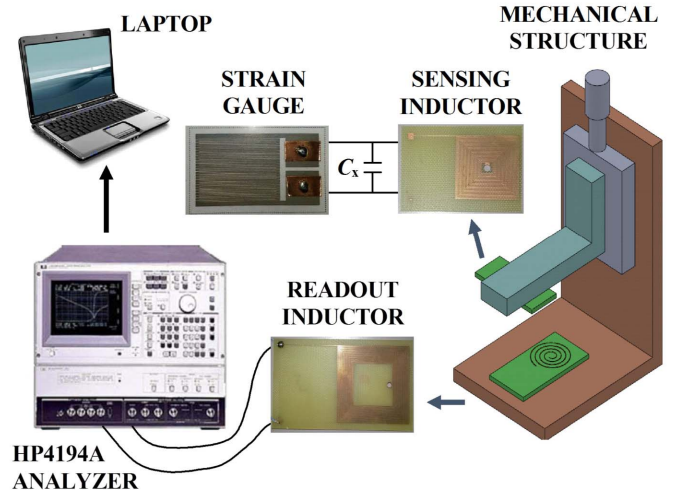


Fig. 6. Scheme of the used experimental setup.

structure whose axes are moved by micrometric screws (which have a resolution of 10 μm). Such an assembly permitted to maintain the two planar spirals parallel and coaxial. Finally, we connected readout inductor's terminals to HP4194A analyzer, which was controlled by an algorithm executed on laptop for data acquisition and elaboration. Analyzer and laptop formed system readout unit. We measured sensor's current with the used setup in this configuration. Its RMS value was 10 μA , corresponding to a power consumption of 16 nW.

Measurement protocol included the following steps. First, printed strain gauge was left at rest position, and laptop drove HP4194A to perform a frequency sweep from 1.7 to 2.2 MHz (these limits define interval Δf_2 for the used device) and read system impedance. The algorithm identified the value φ_0 of phase at frequency f_{res} and calculated parameter β , by implementing (7), starting from inductors' equivalent elements, capacitance C_x , and sensor output $R_{x,0}$, which are already known. Afterward, we put the system in continuous operation, beginning the true measurement procedure. During a cycle of 4 s, HP4194A executed a sweep in the same frequency range, laptop acquired impedance data, and the algorithm found phase φ and calculated sensor output by implementing (6), using system elements and parameter β previously obtained. While program was working, we applied increasing pulling forces on the sensor, in order to induce incremental strain levels of about 0.25%, 0.5%, 0.75%, and 1% of its length at rest, and we kept the corresponding reached positions for few minutes. Furthermore, we saved all data for further offline elaboration.

IV. RESULTS AND DISCUSSION

A. Impedance Analysis

This section reports the results found from the analysis of acquired impedance data. Fig. 7 (top) and (bottom) presents some of the obtained curves representing impedance magnitude and phase, respectively. Each curve corresponds to a different value of applied strain. It should be noted that they reflect the trends within interval Δf_2 shown in Fig. 2. Three insets highlight the ranges close to the points most

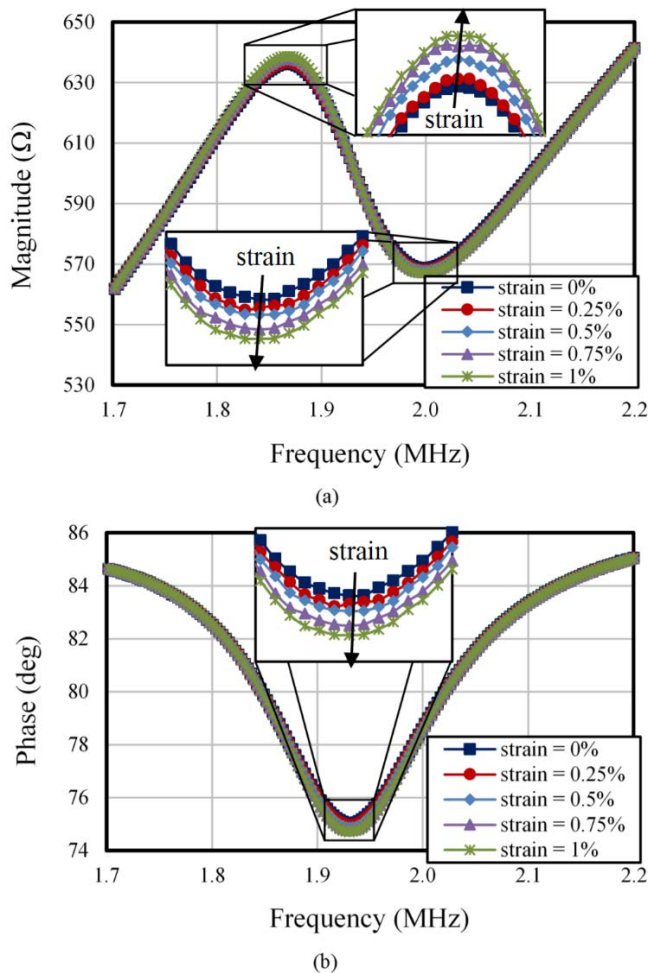


Fig. 7. Curves of system impedance as a function of frequency, for different values of applied strain, with insets highlighting the ranges close to the points most sensitive to strain variation. (a) Magnitude. (b) Phase.

sensitive to strain variation. These graphs are analogous to the curves reported in [15], confirming what we found in the previous work, i.e., such points become more pronounced as strain increases. In particular, phase dip grows, as already pointed out in Fig. 3. Furthermore, Fig. 7 shows how measured sensor current level still permitted to read a stable impedance signal.

Then, we analyzed how much f_{\min} changed when strain increased from 0% to 1% of sensor length at rest. We found that it decreased of 700 Hz on average (i.e., 0.03%) with respect to the initial condition. This confirms that neglecting such an change is an acceptable hypothesis. Furthermore, we investigated the influence of readout unit performances on f_{\min} stability. For a given value of strain, we estimated an experimental uncertainty of about 500 Hz, for a 99% CI.

Frequency variability is reflected in the corresponding amplitude points. Fig. 8 focuses on phase φ , by presenting its variation over time, for the entire test duration. This graph permits to recognize single steps, corresponding to a specific strain value (which is reported in Fig. 8). Phase at f_{res} passes from about 75.05° (in the case of no strain) to about 74.70° at the end of measurement period, resulting in an average decrease of about 0.35° .

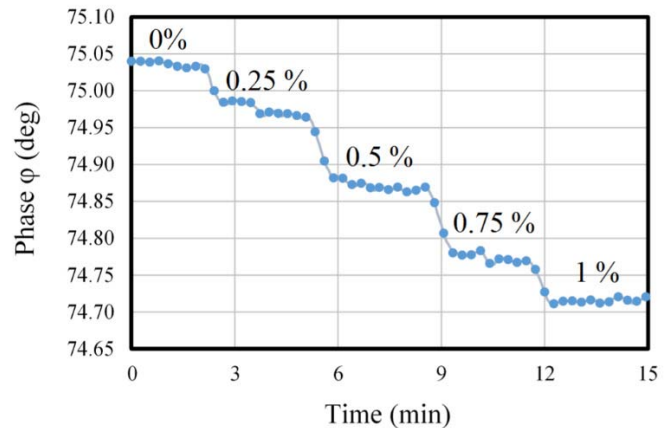


Fig. 8. Variation of phase φ over time, during the experimental analysis. Each value of applied strain is reported above the corresponding level.

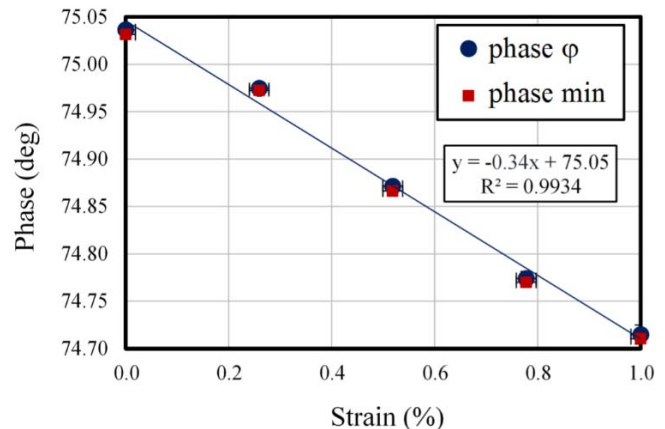


Fig. 9. Phase φ , with its linear regression, and phase minimum, as functions of applied strain.

Variation of φ can also be verified from Fig. 9, which reports it as a function of strain. Fig. 9 helps to appreciate how its trend is almost linear within the considered strain range; in fact, a regression line fits the points with a coefficient of determination R^2 greater than 0.99. Furthermore, we compared such a series with that of phase minimum. Points are very close to each other. Indeed, they differ by 0.006%, for all strain values. This means that using φ instead of phase minimum in the proposed measurement procedure does not affect system sensitivity to strain variation. On the other hand, a distance between the inductors equal to 15 mm is sufficient for the used system to satisfy the assumptions presented in [25] about f_{\min} identification. In addition, Fig. 9 permits to conclude that phase minimum variation is greater than the one detected in [15]. This was predictable, since used sensor has a greater gauge factor (therefore, R_x change is bigger). Finally, phase deviation from average is limited. In fact, we obtained a maximum uncertainty equal to 0.004° , for a 99% CI. Such variability is acceptable for our case, since strain range we are investigating requires to measure phase with accuracy and resolution around the hundredth of degree.

We also evaluated the effects on phase of a distance deviation around the considered value of 15 mm. We moved

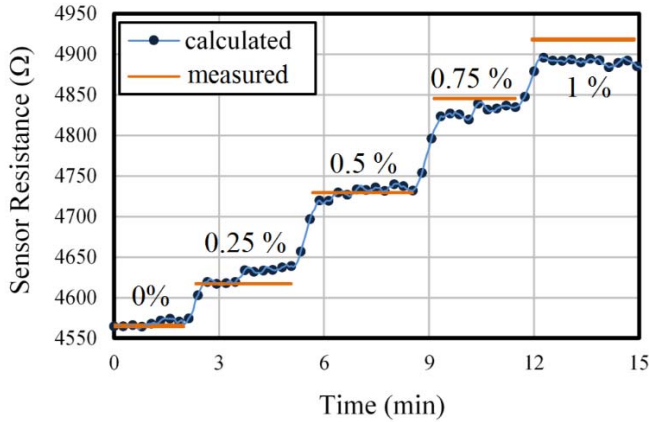


Fig. 10. Time trend of sensor resistance calculated through the proposed measurement method, during the experimental analysis. It is compared with measured values obtained from studying strain gauge behavior. Each value of applied strain is reported above the corresponding level.

mechanical structure axes through its micrometric screws. We estimated a variation of 0.01° every $10 \mu\text{m}$ of distance change. This means that a maximum deviation of few micrometers is tolerated.

System implementation to a real application would require replacing HP4194A analyzer with a low-cost electronic circuit for phase measurement. The literature shows different solutions [28]–[34]. A first option consists in acquiring signal real and imaginary parts using direct digital synthesizers (DDS) and transimpedance amplifiers, and then calculating the phase through trigonometric relationships. However, it is necessary to carefully match in-phase and quadrature references, which otherwise can cause large phase errors. In [28], this solution allowed achieving an operating frequency stability comparable with that obtained with HP4194A analyzer. Therefore, we think that it could meet phase requirements for our system. Then, the employment of DDS combined with code-division multiplexing [31] permitted to measure phase with an accuracy of the hundredth of degree. An alternative involves the use of a phase-locked loop, which can provide accuracies close to one thousandth of degree. In these configurations, attention must be paid when the frequency range is in the order of megahertz. Finally, magnitude ratio and phase difference detection methods could represent a valid possibility as well [34].

B. Strain Measurement

This section includes the achievements regarding strain calculation through the proposed method and discusses how the technique is effective in pursuing this goal. Fig. 10 shows time trend of calculated sensor resistance, compared with that obtained from the evaluation of sensor behavior. R_x variation found through the method is characterized by successive steps, consequent to the increasing applied strain (whose entity is reported in Fig. 10). This reflects phase behavior illustrated in Fig. 8. Furthermore, Fig. 10 permits us to appreciate how calculated resistance follows measured levels.

Fig. 11 provides additional information for method evaluation. It includes values of calculated strain, together with error bars representing its experimental standard deviation, as

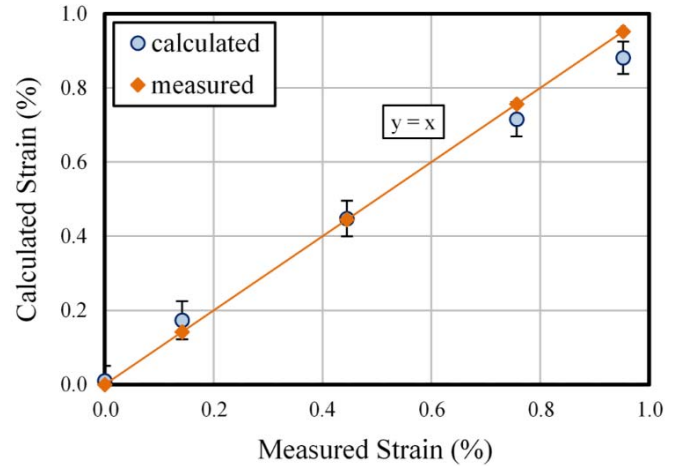


Fig. 11. Calculated strain (identified by series “calculated”) as a function of measured strain, compared with “measured” series.

a function of measured points, derived from the analysis of sensor behavior. We found strain from calculated sensor resistance by considering the gauge factor reported in Section III. Standard deviation permits us to estimate a maximum uncertainty on calculated strain equal to 0.02% of sensor length at rest, for a 99% CI. Furthermore, Fig. 11 compares these points with “measured” series, representing the ideal case in which calculated values are exactly equal to the measured ones. Fig. 11 confirms what we achieved in Fig. 10, pointing out how strain derived from the proposed technique is a valid estimation of the reference case. We found percentage deviation $\%dev$ between the two series, defined as

$$\%dev = \frac{\varepsilon_{\text{meas}} - \varepsilon_{\text{calc}}}{\varepsilon_{\text{meas}}} \cdot 100 \quad (8)$$

where $\varepsilon_{\text{meas}}$ and $\varepsilon_{\text{calc}}$ are the measured and calculated values of strain, respectively. It goes between 0.7% (in the best case) and 7% (in the worst case). Thus, the proposed method holds the potential of achieving an accuracy of the same order as other devices shown in the literature. For instance, [12] reports fiber Bragg grating sensors measuring strain with errors of less than $10 \mu\varepsilon$, whereas our solution arrives to $30 \mu\varepsilon$ in the best case. Although the proposed design does not allow achieving superior performances, in terms of accuracy, than the best devices that are currently used, it guarantees wireless and batteryless measurements, which could be a fundamental aspect to consider when choosing a system for a specific application. The proposed design could present advantages in terms of costs too. It could be less expensive than current technologies, if also considering the adoption of low-cost inkjet-printing technology. Finally, sensor power consumption is low, as seen from current measurement. However, values reported in Section III-C could be even smaller, since components with different characteristics and power requirements could be used in real cases, depending on the application. Furthermore, sensing circuit can be interrogated in an intermittent way, if on-demand strain detection is required, rather than a continuous monitoring. In this case, problem regarding self-heating due to power dissipation would be negligible.

V. CONCLUSION

This paper has proposed a technique for wireless measurement of strain through telemetric systems operating with resistive sensors fabricated with the innovative inkjet-printing technology. It is based on the implementation of mathematical formulas that allow calculating sensor output in an analytical way starting from system parameters and a measure of impedance phase performed at readout inductor terminals at the frequency identifying sensing inductor resonance. The proposed method was validated through an experimental analysis, by applying a progressively increasing strain on a telemetric device made of a low-cost inkjet-printed sensor and PCB planar inductors. Achieved results are promising. They demonstrate that low-cost inkjet-printed components are instruments effective in carrying out the tasks for which they are manufactured. On the other side, the presented technique can be a viable solution that can be applied in situations where strain detection cannot be correctly performed with traditional devices, because of the characteristics of measurement environment. Furthermore, the proposed system permits wireless and batteryless measurements, and is a low-power and low-cost solution.

Anyway, there is a certain margin for further studies. For instance, the problem concerning the distance between the inductors could be faced. In fact, we kept it fixed during the activity, since we developed the technique for this case. However, we are working on the introduction of a trick for compensating distance variations larger than the quantity tolerated now (as proposed in [19] for systems using capacitive sensors), to guarantee results independent from such variable and extend method implementation to applications that require inductors to move from each other. Furthermore, the definition of a proper readout unit could be tackled, by replacing the impedance analyzer used for method validation with a low-cost electronic circuit, according to one of the alternatives proposed in the previous section.

REFERENCES

- [1] A. Deivasigamani, A. Daliri, C. H. Wang, and S. John, "A review of passive wireless sensors for structural health monitoring," *Modern Appl. Sci.*, vol. 7, no. 2, pp. 57–76, Jan. 2013.
- [2] W. Wang, T. Liu, H. Ge, and M. Liu, "Strain measurement based on microstrip patch antennas," in *Proc. RAMS*, Palm Harbor, FL, USA, Jan. 2015, pp. 1–6.
- [3] R. Matsuzaki and A. Todoroki, "Wireless strain monitoring of tires using electrical capacitance changes with an oscillating circuit," *Sens. Actuators A, Phys.*, vol. 119, no. 2, pp. 323–331, 2005.
- [4] H. Cao *et al.*, "Development and characterization of a novel interdigitated capacitive strain sensor for structural health monitoring," *IEEE Sensors J.*, vol. 15, no. 11, pp. 6542–6548, Nov. 2015.
- [5] H. Nakamoto, H. Ootaka, M. Tada, I. Hirata, F. Kobayashi, and F. Kojima, "Stretchable strain sensor with anisotropy and application for joint angle measurement," *IEEE Sensors J.*, vol. 16, no. 10, pp. 3572–3579, May 2016.
- [6] F. Umbrecht *et al.*, "Wireless implantable passive strain sensor: Design, fabrication and characterization," *J. Micromech. Microeng.*, vol. 20, no. 8, p. 085005, 2010.
- [7] H. Cao *et al.*, "A wireless strain sensor system for bladder volume monitoring," in *IEEE MTT-S Int. Microw. Symp. Dig.*, Baltimore, MD, USA, Jun. 2011, pp. 1–4.
- [8] W. C. de Jong, J. H. Koolstra, L. J. van Ruijven, J. A. M. Korfage, and G. E. J. Langenbach, "A fully implantable telemetry system for the long-term measurement of habitual bone strain," *J. Biomech.*, vol. 43, no. 3, pp. 587–591, 2010.
- [9] S. Kon and R. Horowitz, "A high-resolution MEMS piezoelectric strain sensor for structural vibration detection," *IEEE Sensors J.*, vol. 8, no. 12, pp. 2027–2035, Dec. 2008.
- [10] T. Kobayashi, T. Yamashita, N. Makimoto, S. Takamatsu, and T. Itoh, "Ultra-thin piezoelectric strain sensor 5×5 array integrated on flexible printed circuit for structural health monitoring by 2D dynamic strain sensing," in *Proc. MEMS*, Shanghai, China, Jan. 2016, pp. 1030–1033.
- [11] J. Xu and H. Jo, "Development of high-sensitivity and low-cost electroluminescent strain sensor for structural health monitoring," *IEEE Sensors J.*, vol. 16, no. 7, pp. 1962–1968, Apr. 2016.
- [12] K. Bhowmik *et al.*, "High intrinsic sensitivity etched polymer fiber Bragg grating pair for simultaneous strain and temperature measurements," *IEEE Sensors J.*, vol. 16, no. 8, pp. 2453–2459, Apr. 2016.
- [13] C. Shen, C.-P. Wang, M. Sanghadasa, and L. Lin, "Direct-write polymeric strain sensors with arbitrary contours on flexible substrates," in *Proc. MEMS*, Shanghai, China, Jan. 2016, pp. 869–872.
- [14] B. Andò and S. Baglio, "All-inkjet printed strain sensors," *IEEE Sensors J.*, vol. 13, no. 12, pp. 4874–4879, Dec. 2013.
- [15] B. Andò, M. Bona, C. O. Lombardo, E. Sardini, and M. Serpelloni, "Study on a telemetric system that works with an inkjet-printed resistive strain gauge," in *Proc. IEEE SAS*, Catania, Italy, Apr. 2016, pp. 1–4.
- [16] D. Marioli, E. Sardini, M. Serpelloni, and A. Taroni, "Contactless transmission of measurement information between sensor and conditioning electronics," *IEEE Trans. Instrum. Meas.*, vol. 57, no. 2, pp. 303–308, Feb. 2008.
- [17] Y. Jia, K. Sun, F. J. Agosto, and M. T. Quiñones, "Design and characterization of a passive wireless strain sensor," *Meas. Sci. Technol.*, vol. 17, no. 11, pp. 2869–2876, 2006.
- [18] J. C. Butler, A. J. Vigliotti, F. W. Verdi, and S. M. Walsh, "Wireless, passive, resonant-circuit, inductively coupled, inductive strain sensor," *Sens. Actuators A, Phys.*, vol. 102, nos. 1–2, pp. 61–66, Dec. 2002.
- [19] D. Marioli, E. Sardini, M. Serpelloni, and A. Taroni, "A new measurement method for capacitance transducers in a distance compensated telemetric sensor system," *Meas. Sci. Technol.*, vol. 16, no. 8, pp. 1593–1599, 2005.
- [20] B. Andò, "Inkjet printing: A real opportunity for the next generation of low-cost sensors," *IEEE Instrum. Meas. Mag.*, vol. 16, no. 3, pp. 44–48, Jun. 2013.
- [21] W. Su, B. Cook, M. Tentzeris, C. Mariotti, and L. Roselli, "A novel inkjet-printed microfluidic tunable coplanar patch antenna," in *Proc. IEEE APSURSI*, Memphis, TN, USA, Jul. 2014, pp. 858–859.
- [22] H. Andersson, A. Manuilskiy, T. Unander, C. Lidenmark, S. Forsberg, and H.-E. Nilsson, "Inkjet printed silver nanoparticle humidity sensor with memory effect on paper," *IEEE Sensors J.*, vol. 12, no. 6, pp. 1901–1905, Jun. 2012.
- [23] S. Cruz, D. Dias, J. C. Viana, and L. A. Rocha, "Inkjet printed pressure sensing platform for postural imbalance monitoring," *IEEE Trans. Instrum. Meas.*, vol. 64, no. 10, pp. 2813–2820, Oct. 2015.
- [24] B. Andò, S. Baglio, V. Marletta, and A. Pistorio, "A contactless inkjet printed passive touch sensor," in *Proc. IEEE I2MTC*, Montevideo, Uruguay, May 2014, pp. 1638–1642.
- [25] M. A. Fonseca, J. M. English, M. von Arx, and M. G. Allen, "Wireless micromachined ceramic pressure sensor for high-temperature applications," *J. Microelectromech. Syst.*, vol. 11, no. 4, pp. 337–343, Aug. 2002.
- [26] U.-M. Jow and M. Ghovanloo, "Design and optimization of printed spiral coils for efficient transcutaneous inductive power transmission," *IEEE Trans. Biomed. Circuits Syst.*, vol. 1, no. 3, pp. 193–202, Sep. 2007.
- [27] B. Andò, S. Baglio, S. La Malfa, and G. L'Episcopo, "All inkjet printed system for strain measurement," in *Proc. IEEE Sensors*, Limerick, Ireland, Oct. 2011, pp. 215–217.
- [28] E. Sardini and M. Serpelloni, "Wireless measurement electronics for passive temperature sensor," *IEEE Trans. Instrum. Meas.*, vol. 61, no. 9, pp. 2354–2361, Sep. 2012.
- [29] R. Pallás-Areny and J. G. Webster, *Sensors and Signal Conditioning*, 2nd ed. Hoboken, NJ, USA: Wiley, 2001.
- [30] P. Kassanos, I. F. Triantis, and A. Demosthenous, "A CMOS magnitude/phase measurement chip for impedance spectroscopy," *IEEE Sensors J.*, vol. 13, no. 6, pp. 2229–2236, Jun. 2013.
- [31] M. Gevers, P. Gebhardt, S. Westerdick, M. Vogt, and T. Musch, "Fast electrical impedance tomography based on code-division-multiplexing using orthogonal codes," *IEEE Trans. Instrum. Meas.*, vol. 64, no. 5, pp. 1188–1195, May 2015.

- [32] M. I. Bellotti, D. Dellavale, and F. J. Bonetto, "A new technique to detect ocular pathologies based on electrical measurement implemented on programmable logic," *IEEE Trans. Instrum. Meas.*, vol. 61, no. 12, pp. 3290–3294, Dec. 2012.
- [33] E. Pinotti and E. Puppini, "Simple lock-in technique for thickness measurement of metallic plates," *IEEE Trans. Instrum. Meas.*, vol. 63, no. 2, pp. 479–484, Feb. 2014.
- [34] A. S. Anusha, S. P. Preejith, J. Joseph, and M. Sivaprakasam, "Design and preliminary analysis of a multifrequency bioimpedance measurement scheme," in *Proc. IEEE MeMeA*, Benevento, Italy, May 2016, pp. 1–6.



Michele Bona was born in Brescia, Italy, in 1989. He received the B.S. and M.S. degrees (*summa cum laude*) in industrial automation engineering from the University of Brescia, Brescia, in 2011 and 2013, respectively, where he is currently pursuing the Ph.D. degree with the Department of Information Engineering.

His current research interests include the study of measurement systems exploiting telemetric techniques.



Mauro Serpelloni (M'12) was born in Brescia, Italy, in 1979. He received the M.S. degree (*summa cum laude*) in industrial management engineering and the Ph.D. degree in electronic instrumentation from the University of Brescia, Brescia, in 2003 and 2007, respectively.

He was involved in the design, modeling, and fabrication of measurement systems for industrial applications. He is currently an Assistant Professor of Electrical and Electronic Measurements with the Department of Information Engineering, University of Brescia. His current research interests include biomechatronic systems, contactless transmission between sensors and electronics, contactless activation for resonant sensors, and signal processing for microelectromechanical systems.



Emilio Sardini (M'99) was born in Mantova, Italy, in 1958. He received the M.S. degree in electronics engineering from the Politecnico di Milano, Milan, Italy, in 1983.

Since 1984, he has been conducting research and teaching activities with the Department of Electronics for Automation, University of Brescia, Brescia, Italy, where he has been a Full Professor of Electrical and Electronic Measurements and the Deputy Dean of the Engineering Faculty since 2006. He is currently the Coordinator of the "Technology for Health" Ph.D. Program, the Director of the Department of Information Engineering, and a member of the Academic Senate with the University of Brescia. He has authored or coauthored over 100 scientific papers. His research focused on electronic instrumentation, sensors, and signal conditioning electronics. His current research interests include the development of autonomous sensors for biomedical applications.



Cristian O. Lombardo received the M.S. degree from the University of Catania, Catania, Italy.

He is currently a temporary Research Fellow with the Department of Electric, Electronic and Information Engineering, University of Catania. His current research interests include the sensor design and characterization of sensors, inkjet-printed sensors, and multisensor architectures for AAL.



Bruno Andò (M'97–SM'13) was born in Catania, Italy, in 1969. He received the M.S. degree in electronic engineering and the Ph.D. degree in electrical engineering from the University of Catania, Catania, in 1994 and 1999, respectively.

He has been with the Department of Electric, Electronic and Information Engineering, University of Catania, since 1999, where he is currently an Associate Professor of Sensors and Advanced Instrumentation. His current research interests include the sensor design and optimization, inkjet-printed sensors, energy harvesting, smart materials, multisensor architectures for environmental monitoring and AAL, and nonlinear signal processing.